Boosting the Seebeck Coefficient for Organic Coordination Polymers: Role of Doping-Induced Polaron Band Formation

Yunpeng Liu, Wen Shi, Tianqi Zhao, Dong Wang,* and Zhigang Shuai*

MOE Key Laboratory of Organic OptoElectronics and Molecular Engineering, Department of Chemistry, Tsinghua University, Beijing 100084, People's Republic of China

S *Supporting Information*

ABSTRACT: Organic polymers are becoming emerging thermoelectric materials. Tremendous progress has been achieved for p-type doping, but efficient n-type organic materials are still rare. By investigating potassium-doped n-type poly(nickel-ethyl-enetetrathiolate) using density functional theory coupled with Boltzmann transport equation, we find that (i) formation of the electron polaron band (EPB) split from the conduction band (CB) dominates electron transport; (ii) at low doping concentration, the upper CB gets involved in transport in addition to the EPB as the temperature rises, leading to a highly elevated Seebeck coefficient and power factor; and (iii) at even higher temperature, because the CB starts to dominate, the Seebeck coefficient levels off and then decreases with temperature. Such an "exotic" nonmonotonic temperature effect has been found in experiment but has never been explained. We find that such behavior is primarily due to a polaron effect. A doping-induced polaron band can be employed to boost the Seebeck coefficient, making the organic coordination polymer a peculiar n-type thermoelectric material.
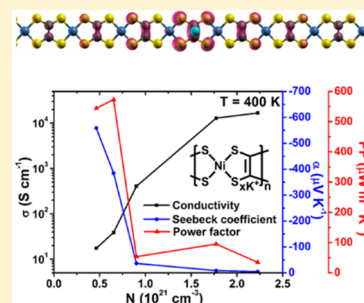
As a green energy solution to waste heat recycling, thermoelectrics have been gaining renewed attention.[1−5] However, the low energy conversion efficiency has limited their application.[3] The performance of thermoelectric materials is evaluated by the figure of merit $zT = \frac{\alpha^2 \sigma T}{\kappa_e + \kappa_L}$, where α is the Seebeck coefficient, σ is the electrical conductivity, T is the absolute temperature, and κ_e and κ_L are electronic and lattice thermal conductivities, respectively. Therefore, the effective way to improve the performance of thermoelectric materials is to increase the Seebeck coefficient and conductivity of the material and reduce the total thermal conductivity. Nevertheless, this is often challenging because these parameters are coupled with each other.[1]

The development of organic thermoelectric materials (OTEs) has advanced rapidly in recent years. Compared with inorganic materials, OTEs have the advantages of low cost, low toxicity, and low thermal conductivity.[6] Owing to their low electrical conductivity, doping is usually needed to improve the thermoelectric performance. By virtue of the careful control of the doping level and removal of ineffective dopants, zT values of 0.25 and 0.42 have been achieved in tosylate (Tos)- and polystyrene sulfonic acid (PSS)-doped poly(3,4-ethylenedioxythiophene) (PEDOT), respectively.[7,8] This makes PEDOT by far the best p-type OTE. The development of n-type OTEs has also made significant progress. Poly(nickel-ethylenetetrathiolate) (poly[Ni-ett]), a metal coordination polymer first synthesized by Poleschner et al.,[9] has been found to be a high-performing n-type OTE.[10−14] In 2016, a zT of 0.32 was reported for potassium-doped poly[Ni-ett] prepared by electrochemical deposition,[13] which is so far record-high among n-type OTEs.

However, understandings toward the role dopants played in optimizing the performance of OTEs are far from satisfactory. In contrast to inorganic thermoelectric materials, OTEs are soft and flexible; therefore, the dopants not only inject charge carriers to the host materials, they may also affect the conduction of charge carriers via altering the packing structure of the host and scattering with the charge carriers. Crispin et al. showed that p-doping of PEDOT with a Tos counterion altered the electronic structure of the polymer via bipolaron formation. The formation of bipolaron band makes PEDOT:-Tos a semimetal, which is the origin of the large Seebeck coefficient observed.[15,16] Previously, we studied the effect of doping on the thermoelectric properties of PEDOT[17] by explicitly including Tos counterions and their scattering to charge carriers in the model. The scattering, which arises from the screened Coulomb interactions between the charges on PEDOT and the counterions, has been ascertained to play a dominant role in the thermoelectric transport of PEDOT:Tos. Recent studies of thermoelectric coordination polymers by Yang et al. were based on the rigid band model.[18−20] In this work, we utilize an explicit doping model to uncover the doping effect on the thermoelectric properties of potassium-doped n-type poly[Ni-ett]. We observed the significant band structure change owing to polaron formation on the polymer chain in poly[K(Ni-ett)$_n$] (shortened to $K_1 Ni_n$ hereafter). The electron polaron band (EPB) split from the conduction band (CB) shows much lower carrier mobility than the CB and

dominates the n-type transport for both the electrical conductivity and Seebeck coefficient at low temperature. As the temperature rises, charge carriers in lightly doped K_1Ni_{14} and K_1Ni_{20} can be thermally activated from the EPB to CB, boosting the Seebeck coefficient and power factor to anomalously large values. At further higher temperature, the CB takes over and the Seebeck coefficient starts to decline. Such abnormal temperature behavior of the Seebeck coefficient, previously observed in experiment,[13] is discussed with the concept of transport entropy and has been attributed to polaron formation in conducting polymers.

Because the intrachain electronic coupling constitutes the major electron conduction pathway of poly[Ni-ett],[13,21] here we set up a one-dimensional model for the crystalline domain of the material, which was manifested to exist by the grazing-incidence X-ray diffraction (GIXRD) result.[13] Structural optimizations and electronic structure calculations were then carried out using the Vienna Ab initio Simulation Package (VASP)[22] with the LDA+U (U = 6.04 eV) functional.[23,24] The optimized cell length of pristine poly[Ni-ett] (along the polymer chain, a axis) is 5.85 Å, which is very close to the experimental value of 5.95 Å.[25] Optimized potassium-doped polymers, K_1Ni_n, show that the K atom is located on top of the C−C bond, which is in accordance with the structural model proposed by Vogt et al. based on the experimental analysis.[26] The doping level is denoted by $1/n$ and usually less than 100%;[12,13,25−28] therefore, we take n from 1 to 20 to represent various doping levels.

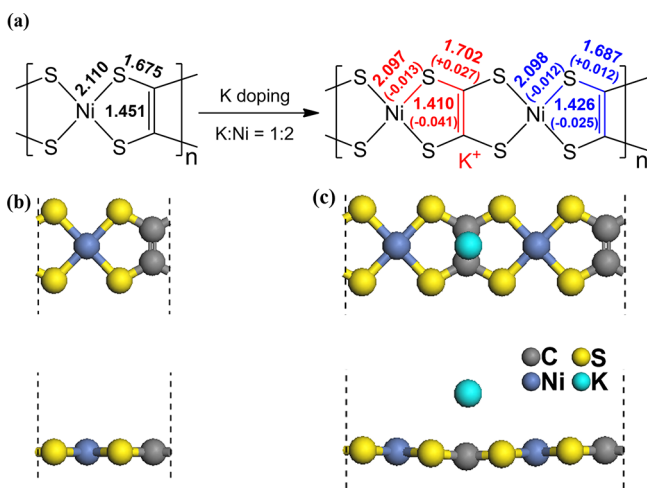We identify a structural transformation of the polymer backbone after doping upon charge injection (Figure 1a).[28]

Figure 1. (a) Chemical structure of pristine poly[Ni-ett] and poly[K(Ni-ett)$_2$]. The lengths of C−C, C−S, and Ni−S bonds (in unit of Å) are given. The bond length change (in unit of Å) after doping (in poly[K(Ni-ett)$_2$]) is shown in parentheses as well. (b) Top and side views of optimized pristine poly[Ni-ett] in a unit cell. (c) Top and side views of poly[K(Ni-ett)$_2$] in a unit cell. The color code for atoms is gray for C, yellow for S, blue for Ni, and cyan for K.

Around 0.88 electrons are transferred from potassium to the polymer backbone based on Bader's charge analysis. The C−S bond is elongated, and the C−C bond is shortened (Figure 1a). The structural transformation is only observed in bonds close to K$^+$. Such a localized change of bond length indicates the formation of polarons due to Coulomb interactions between the charge on the polymer backbone and counterion,

K^+, as reported in previous theoretical studies of other polymers including PEDOT, polythiophene, and polypyrrole.[29−31]

The pristine poly[Ni-ett] is a semiconductor with a direct band gap of 0.42 eV at the Γ point, with a conduction bandwidth of 1.32 eV (Figure 2a). The partial density of states (pDOS) shows that p orbitals of C, S, and Ni as well as d orbitals of Ni constitute the CB (Figure 2a), forming a π−d conjugation system. After K-doping, the CB splits into a series of narrow bands, and the bandwidth of the lowest one decreases dramatically with an increasing number of nickel atoms n (Figure 2e). According to the pDOS (Figure 2a−d), the composition of bands barely changes after splitting, indicating that the band narrowing in doped polymers is not caused by participation of dopant orbitals. Actually, K orbitals do not contribute to these bands. The electron density distribution at the Fermi level, as shown in Figure 2f, clearly demonstrates the charge localization near K$^+$ in lightly doped polymers, such as K_1Ni_{10}. It is coincident with the localized bond distortion mentioned above, indicating the formation of polarons. According to previous theoretical and experimental research, the polaron arises from both electron−phonon coupling (often manifested by backbone distortion) and the Coulomb interaction between the excess charge and the dopant through the "pinning effect",[29,32−38] which lower the energy of charge carriers. The carriers become self-trapped and polarons are formed when the stabilization energy is large enough.[36] The EPB arises in the forbidden band with a narrow bandwidth due to self-trapping.[38] The EPB here is half-filled, with the Fermi energy lying in the band, which is a marked feature of polaron bands. The other bands split from the pristine CB are normal CBs, which possess better transport properties than the EPB. The energy gap between the EPB and the lowest CB is not large, giving the electrons in the EPB a good chance to be thermally activated to the CB.

The exact size of the polaron, or the charge localization length, can be derived from the inverse participation ratio (IPR),[39] defined as

$$IPR_i = \frac{\sum_j |c_{ij}|^4}{\left(\sum_j |c_{ij}|^2\right)^2}$$

(1)

where c_{ij} denotes the wave function expansion coefficient at site j for the ith crystal orbital. If the wave function is delocalized completely over M sites, IPR = $1/M$. Therefore, the localization length is represented by 1/IPR, and is shown in Figure 2e for K_1Ni_n. With n increasing, it converges to 4.5 monomers. The above analysis reveals a polaron size of 4.5 monomer sites. The polaron bandwidth decreases exponentially with n (Figure 2e) because the polaron coupling (hopping integral) decreases exponentially with the interpolaron distance.

The polaron band narrowing and charge localization effect have significantly strong influences on the thermoelectric properties. The electrical conductivity σ and the Seebeck coefficient α at a temperature of 400 K are shown in Figure 3. The effective cross-sectional area of 5.9 Å × 3.2 Å taken from experiment[13] is applied to convert the conductance to conductivity. The Seebeck coefficients for K_1Ni_{14} and K_1Ni_{20} are substantially larger than those for other polymers. Although the electrical conductivity in lightly doped polymers is low due to the band narrowing and charge localization effect, the power
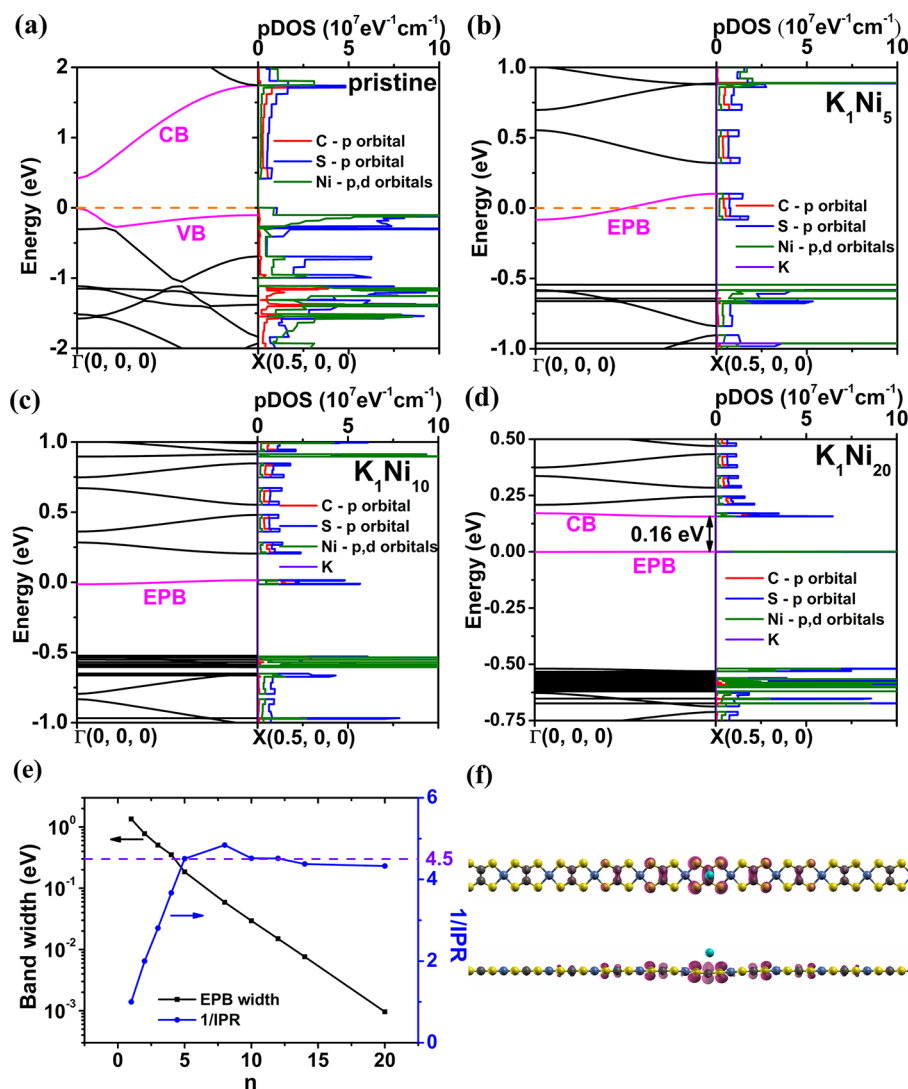
Figure 2. Band structure and pDOS of (a) pristine poly[Ni-ett], (b) K_1Ni_5, (c) K_1Ni_{10}, and (d) K_1Ni_{20}. The CB and valence band (VB) in the pristine poly[Ni-ett], the EPB in the doped polymers, as well as the lowest CB in K_1Ni_{20} are highlighted in pink. The Fermi level is at 0 eV. (e) Electron polaron bandwidth (EPBW) and charge localization length estimated by 1/IPR as a function of n for poly[K(Ni-ett)$_n$]. (f) Charge density distribution (violet red isosurface, top and side views) of EPB in poly[K(Ni-ett)$_{10}$], which shows obvious charge localization near K^+.
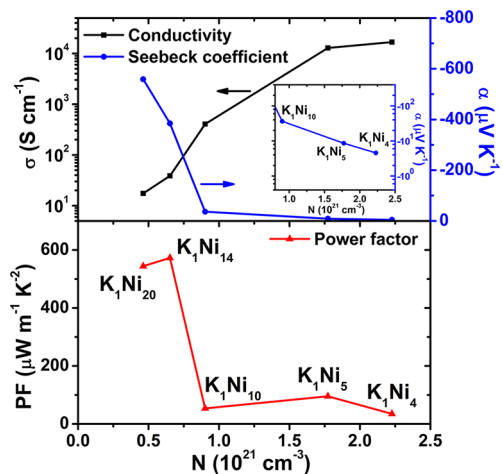

Figure 3. Conductivity, Seebeck coefficient, and power factor as a function of charge density N (at temperature T = 400 K).

factor reaches the peak value at a doping level of n = 14. The conductivity and Seebeck coefficient relation obviously deviates from that derived from the one-band transport model, $\alpha \propto \ln \sigma$ (Figure S5).[40] Herein, we propose a two-band transport model to explain the deviation and the temperature dependence of thermoelectric properties in lightly doped polymers.

Figure 4 shows the charge mobility, conductivity, and Seebeck coefficient for K_1Ni_n as a function of temperature. Two categories are easily demonstrated: those of heavy dopings with $n \leq 5$ exhibit slight temperature dependence, and those of light dopings with n = 14 and 20 show nonmonotonic temperature dependence, which is unusual and will be explained by including both the EPB and CB in charge transport. The turnover in the conductivity–temperature curve (Figure 4a) was observed in experiment on electrochemically doped poly[K$_x$(Ni-ett)].[13] In lightly doped polymers, there exists a small energy gap between the EPB and CB. When the temperature is low, the EPB dominates charge transport, which gives rise to low mobility and conductivity. With the increase of temperature, the ionized impurity scattering, the dominant
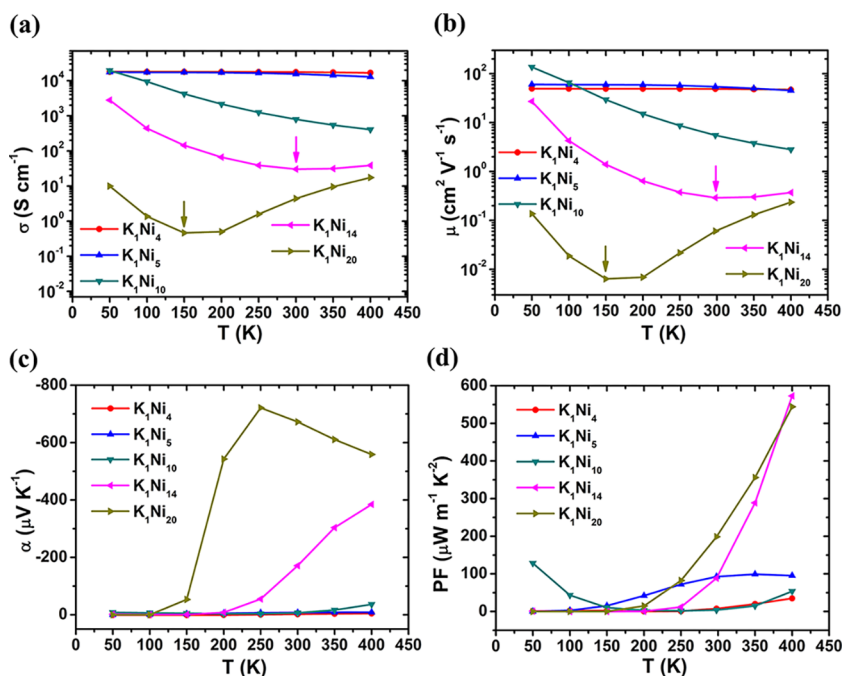
(a)

(b)

(c)

(d)

Figure 4. (a) Electric conductivity, (b) mobility, (c) Seebeck coefficient, and (d) power factor (PF) as a function of temperature for poly[K(Ni-ett)$_n$] at different doping levels. The turning points of electrical conductivity and mobility in K$_1$Ni$_{14}$ and K$_1$Ni$_{20}$ are specifically denoted in the figure.

scattering mechanism here (Figure S6), is enhanced due to the decrease of screening strength (Figure S7), which then leads to the reduction of mobility and conductivity (Figure 4a,b). However, as the temperature rises further, more charge carriers can be thermally activated from the EPB to CB due to the small energy gap between them (e.g., the energy gap is ∼0.16 eV in K$_1$Ni$_{20}$). Because the CB (e.g., the bandwidth is 14.6 meV in K$_1$Ni$_{20}$) is much more dispersed than the EPB (e.g., the bandwidth is 0.96 meV in K$_1$Ni$_{20}$), charge carriers in the CB move faster. Therefore, at higher temperature, both the mobility and conductivity increase.

Sudden increases in the Seebeck coefficient at 250 and 150 K are found in K$_1$Ni$_{14}$ and K$_1$Ni$_{20}$, respectively (Figure 4c), which coincide with the turning points observed in the conductivity−temperature curve, indicating that the CB starts to play a role in charge transport. Surprisingly, the Seebeck coefficient of K$_1$Ni$_{20}$ starts to drop again at 250 K (Figure 4c). According to our calculation, such nonmonotonic temperature dependence of the Seebeck coefficient is due to the two-band transport behavior (see Figure 5 and the corresponding below). Such unusual behavior has been observed in
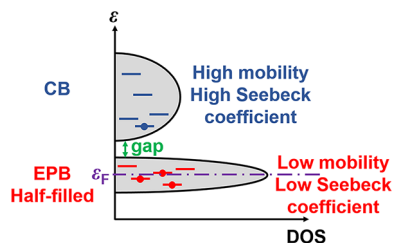
experiment, where the Seebeck coefficient increases with temperature first and then starts to drop at 510 K in electrochemically doped poly[K$_x$(Ni-ett)].[13]

According to the Onsager's reciprocal relations and Kelvin relations, the Seebeck coefficient α can be expressed as the "transport entropy" S divided by the charge of the electron $-e$.[41] This transport entropy consists of three parts: the change of entropy of mixing upon adding a carrier, the change of entropy resulting from the spin degeneracy, and the change of entropy due to the effect of injecting a carrier on molecular vibrations.[38,42] Because the last two terms are not sensitive to the temperature,[38,42] only the change of entropy of mixing is considered when discussing the temperature effect. In the narrow band limit, the entropy of mixing for a system with N_0 states and $N = N_0 f_0$ carriers (where f_0 is the Fermi−Dirac distribution function) can be expressed as

$$S_{mix} = -N_0 k_B[f_0 \ln(f_0) + (1 - f_0) \ln(1 - f_0)] \quad (2)$$

The corresponding Seebeck coefficient is

$$\alpha_{mix} = -\frac{1}{e}\frac{\partial S_{mix}}{\partial N} = -\frac{1}{e}\frac{\partial S_{mix}}{\partial(N_0 f_0)} = -\frac{k_B}{e}\ln\left(\frac{1-f_0}{f_0}\right) \quad (3)$$

Obviously, the Seebeck coefficient is large when the transport band is nearly empty or nearly full-filled. For a half-filled band, $f_0 = 0.5$ and $\alpha_{mix} = 0$. At low temperature, the EPB of K$_1$Ni$_{14}$ and K$_1$Ni$_{20}$ is narrow and half-filled; therefore, the Seebeck coefficient is small. The conclusion that polaron bands have a low Seebeck coefficient was also drawn by Bubnova et al.[15] The sudden increase of Seebeck and anomalously large values at higher temperature can be attributed to the thermal activation of electrons from the EPB to CB. Because the CB is now nearly empty, its Seebeck coefficient is large. Our conclusion that the wide CB possesses a larger Seebeck coefficient than the narrow EPB is not in conflict with Mahan

Figure 5. Schematics of the two-band transport model for K-doped poly[Ni-ett]. The Fermi level ε_F lies in the half-filled EPB. Electrons can be thermally activated from the EPB to CB at high temperature due to the small energy gap.

et al.'s viewpoint that a narrow band benefits the thermo-electric conversion[43] because their deduction is based on the assumption that the two bands have similar electron occupancy f_0, which is however very different for the CB and EPB here. The occupancy of the band is more important to the Seebeck coefficient in our case. In the regime of two-band transport, the total Seebeck coefficient α is the average of α_i (i = EPB, CB) weighted by their contribution σ_i to the total conductivity[38]

$$\alpha = \frac{\alpha_{EPB}\sigma_{EPB} + \alpha_{CB}\sigma_{CB}}{\sigma_{EPB} + \sigma_{CB}} \tag{4}$$

With more carriers activated to the CB at elevated temperature, both σ_{CB} and α increase.

Yet the Seebeck coefficient cannot keep increasing. When the CB dominates the charge transport ($\sigma_{CB} \gg \sigma_{EPB}$), eq 4 is reduced to $\alpha = \alpha_{CB}$, which decreases with temperature and f_0. This explains the drop of α when $T > 250$ K in K_1Ni_{20}.

Overall, the two-band transport model has satisfactorily explained the temperature dependence of thermoelectric properties in lightly doped polymers, highlighting the importance of a polaron-induced charge localization effect in boosting the Seebeck coefficient of K_1Ni_n.

To conclude, we have identified polaron formation in K-doped poly[Ni-ett]. The polaron size is ∼4.5 monomers in the vicinity of K^+; thus, it has been directly observed in lightly doped polymers and has significantly changed the thermo-electric transport behavior. Polaron-induced charge localization causes significant narrowing of the EPB and dramatically reduces the conductivity. Doping can reduce the energy gap between a half-filled EPB and CB, making thermal activation of charge carriers to the much wider CB feasible at higher temperatures. The unusual nonmonotonic temperature dependence of the Seebeck coefficient and its sudden increase for lightly doped K_1Ni_n with n = 14 and 20 can be perfectly explained by polaron band formation coupled with a two-band transport model. The calculated optimal doping level is $1/n$ = 1/14 at 400 K, which is close to the value (∼10%) found in experiment.[12]

■ COMPUTATIONAL DETAILS

Electronic Structure Calculation. Γ-centered k-meshes of $4 \times 1 \times 1$ (pristine and poly[K(Ni-ett)$_n$] with n = 1, 2, 3), $2 \times 1 \times 1$ (n = 4), and $1 \times 1 \times 1$ (n = 5, 8, 10, 12, 14, 20) were used during optimization, while $8 \times 1 \times 1$ (pristine and n = 1, 2, 3, 4), $4 \times 1 \times 1$ (n = 5), and $2 \times 1 \times 1$ (n = 8, 10,12, 14, 20) were used for single-point energy and charge density calculations. Band energies on fine Monkhorst−Pack k-meshes of $300 \times 1 \times 1$ (K_1Ni_4), $240 \times 1 \times 1$ (K_1Ni_5), $120 \times 1 \times 1$ (K_1Ni_{10}), $80 \times 1 \times 1$ (K_1Ni_{14}), and $60 \times 1 \times 1$ (K_1Ni_{20}) were used for BoltzTraP calculations.[44] Band energy interpolation of 50 times was applied for all systems.

Relaxation Time Calculation. The electrical conductivities and Seebeck coefficients were calculated based on the Boltzmann transport equation[45] through BoltzTraP code.[44] The relaxation time was obtained through first-principles calculations. Both acoustic phonon scattering and ionized impurity scattering mechanisms were included to account for the charge carrier relaxation, with the former modeled by deformation potential (DP) theory[46] and the latter derived from the Lindhard screening function for Coulomb interaction between the charge carrier and the counterion.[47,48] Assuming that the scatterings are independent, Matthiessen's rule was

applied to get the total relaxation time: $\tau^{-1} = \tau_{ac}^{-1} + \tau_{ion}^{-1}$, where τ_{ac} and τ_{ion} are relaxation times due to acoustic phonon scattering and ionized impurity scattering, respectively. The acoustic phonon relaxation time was obtained by

$$\frac{1}{\tau_{k,ac}} = \frac{2\pi}{\hbar} \sum_{k'} \frac{k_B T E_1^2}{C_a^{1D}} \delta(\varepsilon_k - \varepsilon_{k'})\left(1 - \frac{v_{k'}}{v_k}\right) \tag{5}$$

where ε_k and v_k are the energy and group velocity of electronic state $|k\rangle$, respectively. E_1 is the deformation potential constant, and C_a^{1D} the 1-D elastic constant along the polymer chain (a direction).

The ionized impurity relaxation time is obtained by

$$\frac{1}{\tau_{k,ion}} = \frac{2\pi}{\hbar} \sum_{k'} \left| \frac{V_{e-ion}(q)}{1 + Scr \cdot F(q)} \right|^2 \delta(\varepsilon_k - \varepsilon_{k'})\left(1 - \frac{v_{k'}}{v_k}\right) \tag{6}$$

where

$$V_{e-ion}(q) = -\frac{Ze^2}{2\pi\varepsilon_r\varepsilon_0 L_0} \iint dy\, dz\, K_0(|q|\sqrt{(y-y_0)^2 + (z-z_0)^2})\rho(y,z) \tag{7}$$

$$F(q) \equiv \iint \iint dy\, dy'\, dz\, dz'\, K_0$$
$$\times (|q|\sqrt{(y-y')^2 + (z-z')^2})\rho(y,z)\rho(y',z') \tag{8}$$

$$Scr = \frac{\gamma e^2 n_{1D,e/h}}{2\pi\varepsilon_r\varepsilon_0 k_B T} \tag{9}$$

Here the screening effect caused by the free carriers is considered. $V_{e-ion}(q)$ is the unscreened scattering matrix. $F(q)$ describes the influence of wave vector change q of the charge carriers during scattering on the screening strength. The screening factor Scr reflects the effect of carrier concentration and temperature on the screening strength. (y_0, z_0) and Z, respectively, are the coordinate and charge number of the ionized impurity. e is the elementary charge. ε_r is the relative dielectric constant, and ε_0 is the permittivity of vacuum. L_0 is the unit cell length. K_0 is the zeroth-order modified Bessel function of the second kind. $\rho(y,z) = |\chi(y,z)|^2$ is the charge density distribution in the plane perpendicular to the chain, and $\chi(y,z)$ represents the wave function in the plane perpendicular to the chain. $n_{1D,e/h}$ is the 1D concentration of electrons/holes. The factor

$$\gamma = \frac{g_s}{L_0} \int_{-\pi/L_0}^{\pi/L_0} f_0(1 - f_0)\frac{L_0}{2\pi} dk/n_{1D,e/h}$$

where g_s represents spin degeneracy. A detailed derivation of the ionized impurity relaxation time formula is provided in the Supporting Information.

The deformation potential constant was obtained by a linear fit of the Fermi level shift with the lattice dilation, calibrated by the vacuum level. Bader charge analysis was carried out to get the charge carried by the ionized potassium.[49] The charge on potassium had a similar value of about +0.88 in all doped chains, showing nearly complete charge transfer (Figure S4). We also calculated the relative dielectric constant ε_r of the pristine chain using the VASP software, which was 4.37. The ionic charge and dielectric constant were used for calculation of the ionized impurity scattering time.

ASSOCIATED CONTENT

Ⓢ Supporting Information

The Supporting Information is available free of charge on the ACS Publications website at DOI: 10.1021/acs.jpclett.9b00716.

Band structure, pDOS, charge density of the EPB, deformation potential, elastic constant, and Bader's charge analysis for K-doped poly[K(Ni-ett)$_n$]; conductivity and Seebeck coefficient relationship; derivation of the 1-D ionized impurity scattering matrix element; and temperature-dependent screening in ionized impurity scattering (PDF)

AUTHOR INFORMATION

ORCID Ⓘ

Yunpeng Liu: 0000-0003-2421-8330
Dong Wang: 0000-0002-0594-0515
Zhigang Shuai: 0000-0003-3867-2331

Notes

The authors declare no competing financial interest.

ACKNOWLEDGMENTS

REFERENCES

(1) Snyder, G. J.; Toberer, E. S. Complex thermoelectric materials. *Nat. Mater.* **2008**, *7*, 105−114.

(2) DiSalvo, F. J. Thermoelectric cooling and power generation. *Science* **1999**, *285*, 703−706.

(3) Bell, L. E. Cooling, heating, generating power, and recovering waste heat with thermoelectric systems. *Science* **2008**, *321*, 1457−1461.

(4) Heremans, J. P. Thermoelectricity: The ugly duckling. *Nature* **2014**, *508*, 327−328.

(5) He, J.; Tritt, T. M. Advances in thermoelectric materials research: Looking back and moving forward. *Science* **2017**, *357*, No. eaak9997.

(6) Zhang, Q.; Sun, Y.; Xu, W.; Zhu, D. Organic thermoelectric materials: emerging green energy materials converting heat to electricity directly and efficiently. *Adv. Mater.* **2014**, *26*, 6829−6851.

(7) Kim, G. H.; Shao, L.; Zhang, K.; Pipe, K. P. Engineered doping of organic semiconductors for enhanced thermoelectric efficiency. *Nat. Mater.* **2013**, *12*, 719−723.

(8) Bubnova, O.; Khan, Z. U.; Malti, A.; Braun, S.; Fahlman, M.; Berggren, M.; Crispin, X. Optimization of the thermoelectric figure of merit in the conducting polymer poly(3,4-ethylenedioxythiophene). *Nat. Mater.* **2011**, *10*, 429−433.

(9) Poleschner, H.; John, W.; Hoppe, F.; Fanghänel, E.; Roth, S. Tetrathiafulvalene. XIX. Synthese und Eigenschaften elektronenleitender Poly-Dithiolenkomplexe mit Ethylentetrathiolat und Tetrathiafulvalentetrathiolat als Brückenliganden. *J. Prakt. Chem.* **1983**, *325*, 957−975.

(10) Sun, Y.; Sheng, P.; Di, C.; Jiao, F.; Xu, W.; Qiu, D.; Zhu, D. Organic thermoelectric materials and devices based on p- and n-type poly(metal 1,1,2,2-ethenetetrathiolate)s. *Adv. Mater.* **2012**, *24*, 932−937.

(11) Jiao, F.; Di, C. A.; Sun, Y. M.; Sheng, P.; Xu, W.; Zhu, D. B. Inkjet-printed flexible organic thin-film thermoelectric devices based on p- and n-type poly(metal 1,1,2,2-ethenetetrathiolate)s/polymer composites through ball-milling. *Philos. Trans. R. Soc., A* **2014**, *372*, 20130008.

(12) Sun, Y. H.; Zhang, J. J.; Liu, L. Y.; Qin, Y. K.; Sun, Y. M.; Xu, W.; Zhu, D. B. Optimization of the thermoelectric properties of poly(nickel-ethylenetetrathiolate) synthesized via potentiostatic deposition. *Sci. China: Chem.* **2016**, *59*, 1323−1329.

(13) Sun, Y.; Qiu, L.; Tang, L.; Geng, H.; Wang, H.; Zhang, F.; Huang, D.; Xu, W.; Yue, P.; Guan, Y. S.; Jiao, F.; Sun, Y.; Tang, D.; Di, C. A.; Yi, Y.; Zhu, D. Flexible n-Type High-Performance Thermoelectric Thin Films of Poly(nickel-ethylenetetrathiolate) Prepared by an Electrochemical Method. *Adv. Mater.* **2016**, *28*, 3351−3358.

(14) Menon, A. K.; Uzunlar, E.; Wolfe, R. M. W.; Reynolds, J. R.; Marder, S. R.; Yee, S. K. Metallo-organic n-type thermoelectrics: Emphasizing advances in Nickel-ethenetetrathiolates. *J. Appl. Polym. Sci.* **2017**, *134*, 44402.

(15) Bubnova, O.; Khan, Z. U.; Wang, H.; Braun, S.; Evans, D. R.; Fabretto, M.; Hojati-Talemi, P.; Dagnelund, D.; Arlin, J. B.; Geerts, Y. H.; Desbief, S.; Breiby, D. W.; Andreasen, J. W.; Lazzaroni, R.; Chen, W. M.; Zozoulenko, I.; Fahlman, M.; Murphy, P. J.; Berggren, M.; Crispin, X. Semi-metallic polymers. *Nat. Mater.* **2014**, *13*, 190−194.

(16) Chabinyc, M. Thermoelectric polymers: Behind organics' thermopower. *Nat. Mater.* **2014**, *13*, 119−121.

(17) Shi, W.; Zhao, T. Q.; Xi, J. Y.; Wang, D.; Shuai, Z. G. Unravelling Doping Effects on PEDOT at the Molecular Level: From Geometry to Thermoelectric Transport Properties. *J. Am. Chem. Soc.* **2015**, *137*, 12929−12938.

(18) Yong, X.; Shi, W.; Wu, G.; Goh, S. S.; Bai, S. Q.; Xu, J. W.; Wang, J. S.; Yang, S. W. Tuning the thermoelectric performance of π-d conjugated nickel coordination polymers through metal−ligand frontier molecular orbital alignment. *J. Mater. Chem. A* **2018**, *6*, 19757−19766.

(19) Shi, W.; Wu, G.; Yong, X.; Deng, T.; Wang, J. S.; Zheng, J. C.; Xu, J.; Sullivan, M. B.; Yang, S. W. Orbital-Engineering-Based Screening of π-Conjugated d^8 Transition-Metal Coordination Polymers for High-Performance n-Type Thermoelectric Applications. *ACS Appl. Mater. Interfaces* **2018**, *10*, 35306−35315.

(20) Shi, W.; Wu, G.; Hippalgaonkar, K.; Wang, J. S.; Xu, J.; Yang, S. W. Poly(nickel-ethylenetetrathiolate) and Its Analogs: Theoretical Prediction of High-Performance Doping-Free Thermoelectric Polymers. *J. Am. Chem. Soc.* **2018**, *140*, 13200−13204.

(21) Alvarez, S.; Vicente, R.; Hoffmann, R. Dimerization and Stacking in Transition-Metal Bisdithiolenes and Tetrathiolates. *J. Am. Chem. Soc.* **1985**, *107*, 6253−6277.

(22) Kresse, G.; Furthmuller, J. Efficient iterative schemes for *ab initio* total-energy calculations using a plane-wave basis set. *Phys. Rev. B: Condens. Matter Mater. Phys.* **1996**, *54*, 11169−11186.

(23) Dudarev, S. L.; Botton, G. A.; Savrasov, S. Y.; Humphreys, C. J.; Sutton, A. P. Electron-energy-loss spectra and the structural stability of nickel oxide: An LSDA+U study. *Phys. Rev. B: Condens. Matter Mater. Phys.* **1998**, *57*, 1505−1509.

(24) Zhou, F.; Cococcioni, M.; Marianetti, C. A.; Morgan, D.; Ceder, G. First-principles prediction of redox potentials in transition-metal compounds with LDA+U. *Phys. Rev. B: Condens. Matter Mater. Phys.* **2004**, *70*, 235121.

(25) Garreau de Bonneval, B.; Faulmann, C.; Verelst, M.; Lecante, P.; Malfant, I.; Cassoux, P. Structural study and magnetic properties of new [(Cp*$_2$M)$_x$(NiC$_2$S$_4$)]$_n$ polymer salts. *Synth. Met.* **2003**, *133−134*, 597−599.

(26) Vogt, T.; Faulmann, C.; Soules, R.; Lecante, P.; Mosset, A.; Castan, P.; Cassoux, P.; Galy, J. A LAXS (large angle x-ray scattering) and EXAFS (extended x-ray absorption fine structure) investigation of conductive amorphous Nickel tetrathiolato polymers. *J. Am. Chem. Soc.* **1988**, *110*, 1833−1840.

(27) Faulmann, C.; Cassoux, P.; Vicente, R.; Ribas, J.; Jolly, C. A.; Reynolds, J. R. Conductive Amorphous Metal-Tetrathiolato Polymers: Synthesis of a New Precursor C$_6$O$_2$S$_8$ and Its Derived Polymers, and LAXS Structural Studies. *Synth. Met.* **1989**, *29*, 557−562.

(28) Tkachov, R.; Stepien, L.; Roch, A.; Komber, H.; Hennersdorf, F.; Weigand, J. J.; Bauer, I.; Kiriy, A.; Leyens, C. Facile synthesis of potassium tetrathiooxalate - The "true" monomer for the preparation of electron-conductive poly(nickel-ethylenetetrathiolate). *Tetrahedron* **2017**, *73*, 2250−2254.

(29) Dkhissi, A.; Beljonne, D.; Lazzaroni, R.; Louwet, F.; Groenendaal, L.; Brédas, J. L. Density functional theory and Hartree-Fock studies of the geometric and electronic structure of neutral and doped ethylenedioxythiophene (EDOT) oligomers. *Int. J. Quantum Chem.* **2003**, *91*, 517−523.

(30) Alkan, F.; Salzner, U. Theoretical investigation of excited states of oligothiophene anions. *J. Phys. Chem. A* **2008**, *112*, 6053−6058.

(31) Ullah, H.; Shah, A. U. A.; Bilal, S.; Ayub, K. Doping and Dedoping Processes of Polypyrrole: DFT Study with Hybrid Functionals. *J. Phys. Chem. C* **2014**, *118*, 17819−17830.

(32) Baughman, R. H.; Brédas, J. L.; Chance, R. R.; Elsenbaumer, R. L.; Shacklette, L. W. Structural Basis for Semiconducting and Metallic Polymer Dopant Systems. *Chem. Rev.* **1982**, *82*, 209−222.

(33) Brédas, J. L.; Thémans, B.; Fripiat, J. G.; André, J. M.; Chance, R. R. Highly conducting polyparaphenylene, polypyrrole, and polythiophene chains: An *ab initio* study of the geometry and electronic-structure modifications upon doping. *Phys. Rev. B: Condens. Matter Mater. Phys.* **1984**, *29*, 6761−6773.

(34) Brédas, J. L.; Street, G. B. Polarons, Bipolarons, and Solitons in Conducting Polymers. *Acc. Chem. Res.* **1985**, *18*, 309−315.

(35) Stafström, S.; Brédas, J. L.; Epstein, A. J.; Woo, H. S.; Tanner, D. B.; Huang, W. S.; MacDiarmid, A. G. Polaron lattice in highly conducting polyaniline: Theoretical and optical studies. *Phys. Rev. Lett.* **1987**, *59*, 1464−1467.

(36) Moliton, A.; Hiorns, R. C. Review of electronic and optical properties of semiconducting π-conjugated polymers: applications in optoelectronics. *Polym. Int.* **2004**, *53*, 1397−1412.

(37) Heeger, A. J.; Sariciftci, N. S.; Namdas, N. B. *Semiconducting and Metallic Polymers*; Oxford University Press: Oxford, 2010.

(38) Emin, D. *Polarons*; Cambridge University Press: New York, 2013.

(39) Linares, M.; Hultell, M.; Stafström, S. The effect of lattice dynamics on electron localization in poly-(para-phenylenevinylene). *Synth. Met.* **2009**, *159*, 2219−2221.

(40) Cutler, M.; Mott, N. F. Observation of Anderson Localization in an Electron Gas. *Phys. Rev.* **1969**, *181*, 1336−1340.

(41) Callen, H. B. The Application of Onsager's Reciprocal Relations to Thermoelectric, Thermomagnetic, and Galvanomagnetic Effects. *Phys. Rev.* **1948**, *73*, 1349−1358.

(42) Venkateshvaran, D.; Nikolka, M.; Sadhanala, A.; Lemaur, V.; Zelazny, M.; Kepa, M.; Hurhangee, M.; Kronemeijer, A. J.; Pecunia, V.; Nasrallah, I.; Romanov, I.; Broch, K.; McCulloch, I.; Emin, D.; Olivier, Y.; Cornil, J.; Beljonne, D.; Sirringhaus, H. Approaching disorder-free transport in high-mobility conjugated polymers. *Nature* **2014**, *515*, 384−388.

(43) Mahan, G. D.; Sofo, J. O. The best thermoelectric. *Proc. Natl. Acad. Sci. U. S. A.* **1996**, *93*, 7436−7439.

(44) Madsen, G. K. H.; Singh, D. J. BoltzTraP. A code for calculating band-structure dependent quantities. *Comput. Phys. Commun.* **2006**, *175*, 67−71.

(45) Wang, D.; Shi, W.; Chen, J.; Xi, J.; Shuai, Z. Modeling thermoelectric transport in organic materials. *Phys. Chem. Chem. Phys.* **2012**, *14*, 16505−16520.

(46) Bardeen, J.; Shockley, W. Deformation Potentials and Mobilities in Non-Polar Crystals. *Phys. Rev.* **1950**, *80*, 72−80.

(47) Lindhard, J. On the Properties of a Gas of Charged Particles. *Mater. Fys. Medd. Dan. Vid.* **1954**, *28*, 1−57.

(48) Li, Q.; Das Sarma, S. Collective excitation spectra of one-dimensional electron systems. *Phys. Rev. B: Condens. Matter Mater. Phys.* **1989**, *40*, 5860−5863.

(49) Henkelman, G.; Arnaldsson, A.; Jonsson, H. A fast and robust algorithm for Bader decomposition of charge density. *Comput. Mater. Sci.* **2006**, *36*, 354−360.